

1 **Evaluating Late Cretaceous OAEs and the influence of marine incursions on**
2 **organic carbon burial in an expansive East Asian paleo-lake**

3 **Matthew M. Jones^{a,*}, Daniel E. Ibarra^b, Yuan Gao^c, Bradley B. Sageman^a, David Selby^d, C.**
4 **Page Chamberlain^b, Stephan A. Graham^e**

5 ^aDepartment of Earth and Planetary Sciences, Northwestern University, Evanston, Illinois 60208,
6 USA matthewjones2012@u.northwestern.edu, b-sageman@northwestern.edu

7 ^bDepartment of Earth System Science, Stanford University, Stanford, California 94305, USA
8 danieli@stanford.edu, chamb@stanford.edu

9 ^cState Key Laboratory of Biogeology and Environmental Geology, School of Earth Sciences and
10 Resources, China University of Geosciences, Beijing, China yuangao@cugb.edu.cn

11 ^dDepartment of Earth Sciences, Durham University, Durham, DH1 3LE, UK
12 david.selby@durham.ac.uk

13 ^eDepartment of Geological Sciences, Stanford University, Stanford, California 94305, USA
14 sagraham@stanford.edu

15

16 *Corresponding author e-mail: matthewjones2012@u.northwestern.edu

17

18 Submitted to *Earth and Planetary Science Letters*

19 Category: Letter

20 Abstract

21 Expansive Late Cretaceous lacustrine deposits of East Asia offer unique stratigraphic
22 records to better understand regional responses to global climate events, such as oceanic anoxic
23 events (OAEs), and terrestrial organic carbon burial dynamics. This study presents bulk organic
24 carbon isotopes ($\delta^{13}\text{C}_{\text{org}}$), elemental concentrations (XRF), and initial osmium ratios ($^{187}\text{Os}/^{188}\text{Os}$,
25 Os_i) from the Turonian-Coniacian Qingshankou Formation, a ~5 Ma lacustrine mudstone
26 succession in the Songliao Basin of northeast China. A notable $\delta^{13}\text{C}_{\text{org}}$ excursion ($\sim+2.5\%$) in
27 organic carbon-lean Qingshankou Members 2-3 correlates to OAE3 in the Western Interior Basin
28 (WIB) of North America within temporal uncertainty of high-precision age models. Decreases
29 in carbon isotopic fractionation ($\Delta^{13}\text{C}$) through OAE3 in the WIB and Songliao Basin, suggest
30 that significantly elevated global rates of organic carbon burial drew down pCO_2 , likely cooling
31 climate. Despite this, Os_i chemostratigraphy demonstrates no major changes in global volcanism
32 or weathering trends through OAE3. Identification of OAE3 in a lake system is consistent with
33 lacustrine records of other OAEs (e.g., Toarcian OAE), and underscores that terrestrial
34 environments were sensitive to climate perturbations associated with OAEs. Additionally, the
35 relatively radiogenic Os_i chemostratigraphy and XRF data confirm that the Qingshankou
36 Formation was deposited in a non-marine setting. Organic carbon-rich intervals preserve no
37 compelling Os_i evidence for marine incursions, an existing hypothesis for generating Member
38 1's prolific petroleum source rocks. Based on our results, we present a model for water column
39 stratification and source rock deposition independent of marine incursions, detailing dominant
40 biogeochemical cycles and lacustrine organic carbon burial mechanisms.

41 1. Introduction

42 Upper Cretaceous marine strata preserve evidence for greenhouse warmth on a planet with
43 high pCO₂ (e.g., Pagani et al., 2014) and lacking sustained ice sheets (MacLeod et al., 2013).
44 Oceanic anoxic events (OAEs) are superimposed on this stratigraphic record of excessive
45 warmth, as relatively brief intervals (<1 Ma) of enhanced organic carbon burial in many basins
46 globally (Jenkyns, 2010 and references therein) accompanied by positive stable carbon isotope
47 excursions (CIEs) (Scholle and Arthur, 1980). Precise correlations of terrestrial and marine
48 records are critical for developing a unified Late Cretaceous paleoclimate reconstruction and
49 understanding the terrestrial response to OAEs, as well as for testing hypotheses for the causal
50 mechanisms of OAEs. However, such correlations are complicated in terrestrial basins due to
51 the common occurrence of hiatuses, lateral heterogeneity in lithofacies, and limited
52 biostratigraphic age control. Despite challenges, some workers have employed carbon isotope
53 ($\delta^{13}\text{C}$) chemostratigraphy to identify Mesozoic OAEs in terrestrial strata and assess local
54 paleoclimate responses (e.g., OAE2, Barclay et al., 2010; OAE1a, Ludvigson et al., 2010).
55 Although comparatively rare in the geologic record, lacustrine facies offer promise in
56 reconstructing robust terrestrial paleoclimate records given relatively continuous, expanded
57 mudstone successions. Paleo-lakes are also suitable for testing hypotheses about OAEs'
58 triggering mechanisms, such as accelerated weathering, and for better resolving regional
59 environmental responses (e.g., Toarcian OAE: Xu et al., 2017).

60 In the non-marine Songliao Basin of northeast China, the SK1-S core provides a relatively
61 continuous Late Cretaceous stratigraphic record from lacustrine and fluvial units influenced by
62 local tectonic and climatic conditions (Fig. 1) (Wang et al., 2013). In addition, the organic
63 carbon-rich mudstones of the Turonian-Coniacian Qingshankou Member 1 are primary

64 petroleum source rocks in China's largest and longest producing non-marine oil and gas basin
65 (Feng et al., 2010). As a result, the depositional history of the Qingshankou Formation has been
66 heavily studied and debated, with some authors arguing that episodic incursions of marine waters
67 during Member 1 drove water column stratification in the basin creating conditions favorable to
68 preservation of organic carbon (e.g., Hou et al., 2000). More recently, the sporadic presence of
69 biomarkers typical of marine algae and sponges in Member 1 and lowermost Members 2 and 3
70 (Hu et al., 2015), and pyrite sulfur isotopic records in Member 1 of SK1-S (Huang et al., 2013)
71 have been interpreted as evidence for transient or even prolonged marine connections. However,
72 the marine incursion hypothesis for source rock deposition in Qingshankou Member 1 remains
73 controversial, as paleogeographic reconstructions note considerable distances to the nearest
74 marine waters (>500 km; Yang, 2013) (Fig. 1) and because no well-preserved uniquely marine
75 micro- or macro-fossils have been reported from the Qingshankou Formation in SK1-S (Xi et al.,
76 2016). Others have interpreted a consistently non-marine water body during the deposition of
77 the Qingshankou Formation (Chamberlain et al., 2013).

78 To assess the influence of OAEs and marine incursions on lacustrine organic carbon burial
79 rates in the dominantly terrestrial Songliao Basin (Wang et al., 2016a), we present sedimentary
80 geochemical measurements of the expanded mudstones of the Qingshankou Formation. The new
81 mid-Turonian to late-Coniacian $\delta^{13}\text{C}_{\text{org}}$ records (*this study*; Hu et al., 2015) serve as a test of
82 $\delta^{13}\text{C}_{\text{org}}$ correlation robustness from an East Asian lacustrine basin to the epicontinental marine
83 $\delta^{13}\text{C}_{\text{org}}$ in the North American Western Interior Basin (WIB) (Joo and Sageman, 2014). Utilizing
84 recently updated radioisotopic and astrochronologic age models (Locklair and Sageman, 2008;
85 Wu et al., 2013; Sageman et al., 2014b; Wang et al., 2016b), we identify the Coniacian Oceanic

86 Anoxic Event 3 (OAE3) in Qingshankou Members 2 and 3 and investigate the event in a lake
87 system using geochemical proxies.

88 Coupled with $\delta^{13}\text{C}$ chemostratigraphy, we present an initial osmium isotope ($^{187}\text{Os}/^{188}\text{Os}$
89 denoted as Os_i) chemostratigraphy from the Songliao Basin to test the marine incursion
90 hypothesis. The Os_i data serve as a proxy for marine connectivity and basin restriction (e.g., Du
91 Vivier et al., 2014), since values reflect a mixture of osmium derived from relatively
92 homogenized open marine waters (Gannoun and Burton, 2014), mixing over geologically brief
93 intervals ($\tau < 10$ ka, Oxburgh, 2001; Rooney et al., 2016), and local continental weathered
94 osmium which tends to be more radiogenic (higher Os_i) (Peucker-Ehrenbrink and Ravizza,
95 2000). As a result, lacustrine formations, isolated from the marine osmium reservoir, generally
96 preserve higher Os_i values due to the flux of proximal radiogenic osmium and limited
97 unradiogenic osmium fluxes (e.g., cosmogenic dust and hydrothermal sources) (Poirier and
98 Hillaire-Marcel, 2011; Cumming et al., 2012; Xu et al., 2017), with the caveat that lacustrine
99 basins weathering ophiolitic lithologies preserve more unradiogenic Os_i (Kuroda et al., 2016).
100 Thus, typical basins with a history of marine connections should record more non-radiogenic Os_i
101 when compared to contemporaneous lacustrine basins. To constrain open marine Os_i values
102 during deposition of Qingshankou Member 1, we present time correlative records from Turonian
103 mudstones from the tropical North Atlantic. Furthermore, we interpret Os_i records as one proxy
104 for continental weathering intensity through Qingshankou Members 2 and 3 (OAE3 interval as
105 demonstrated by this study) and other intervals of SK1-S lacking additional evidence for marine
106 incursions. Finally, to characterize marine osmium cycling and potential perturbations across
107 OAE3 (e.g., LIP volcanism, continental weathering), we present a third small Os_i sample set
108 from the Angus Core in the WIB (Denver Basin, Colorado).

109 Additionally, we present trace element (XRF) analyses spanning the Qingshankou Formation
110 to reconstruct bottom-water redox conditions through major events in the lake's evolution, such
111 as source rock deposition in Member 1 and OAE3 in Members 2 and 3, using established
112 interpretive frameworks (Tribovillard et al., 2006; Sageman et al., 2014a). To conclude, we
113 propose a depositional model, independent of marine connections, to characterize lacustrine
114 biogeochemical cycling during accumulation of the Qingshankou Formation. This model
115 provides a footing for future research to further evaluate scenarios for water column stratification
116 and organic carbon deposition in mid-latitude paleo-lakes discussed herein.

117 **2. Geologic materials SK1-S core**

118 The terrestrial Songliao Basin in northeast China preserves a long-lived Jurassic-Cretaceous
119 stratigraphic record in a deep (>5 km) backarc rifted sag basin (Fig. 1) (Graham et al., 2001;
120 Wang et al., 2013; Wang et al., 2016a). An International Continental Drilling Project coring
121 campaign recovered a sedimentary succession spanning the mid-Turonian to Campanian in two
122 overlapping cores (SK1-S and SK1-N) in 2009. Three fluvio-deltaic formations (oldest to
123 youngest: Quantou, Yaojia, Sifangtai) separated by two thick lacustrine formations
124 (Qingshankou, Nenjiang) comprise the succession. A chronostratigraphic framework has been
125 developed for SK1-S based on lithostratigraphy (Gao et al., 2009; Wang et al., 2009), and
126 biostratigraphy of ostracod, charophyte, and, in the lower Nenjiang Formation, foraminifera
127 (Wan et al., 2013; Xi et al., 2016). Recently published high-precision zircon U-Pb dates (Wang
128 et al., 2016b) and astrochronology (Wu et al., 2013) in the Turonian-Coniacian Qingshankou
129 Formation, the stratigraphic focus of this study, provide precise temporal constraints (± 181 ka)
130 necessary for global correlation and the interpretation of proxy data in the context of global
131 climate events such as OAEs. The Qingshankou Formation is sub-divided into the lower 93m-

132 thick organic-rich laminated mudstone in Member 1 (Gao et al., 2009) and the upper 395m-thick
133 undifferentiated grey shales of Members 2 and 3 (Wang et al., 2009).

134 **3. Methods**

135 3.1 Sampling and SK1-S timescale

136 We collected samples from SK1-S for this study at roughly 5-10 m spacing through the
137 upper Quantou, Qingshankou, and lower Yaojia formations from the China University of
138 Geosciences Beijing core repository. For all Qingshankou Formation samples analyzed, we
139 assign numerical ages by anchoring the floating astronomical time scale from SK1-S (Wu et al.,
140 2013) to a CA-ID-TIMS U/Pb zircon dated bentonite horizon (Ash S1705m = 90.97 ± 0.12 Ma;
141 Wang et al., 2016b) (Table A.1). Considering radioisotopic and astrochronologic sources of
142 uncertainty, we calculate ± 181 ka (2σ) precision for the anchored SK1-S time scale (see
143 Appendix for detailed discussion).

144 3.2 Carbon geochemistry

145 We measured samples collected from the SK1-S Core for bulk organic carbon isotope
146 ratios ($\delta^{13}\text{C}_{\text{org}}$), atomic carbon to nitrogen ratios (C/N), weight percent total organic carbon
147 (TOC), and weight percent carbonate at Northwestern University (Appendix). Additionally, we
148 measured a sample set from the Angus Core in the WIB for bulk carbonate carbon isotopes
149 ($\delta^{13}\text{C}_{\text{carb}}$) to calculate $\Delta^{13}\text{C}$ ($\delta^{13}\text{C}_{\text{carb}} - \delta^{13}\text{C}_{\text{org}}$) to approximate changes in carbon isotope
150 fractionation across OAE3 and compare to $\Delta^{13}\text{C}$ in the Songliao Basin (Appendix).

151 3.3 X-ray fluorescence (XRF)

152 Methods outlined in the Appendix are used to measure major and minor trace element
153 concentrations of sample powders.

154 3.4 Initial osmium isotope analysis

155 To measure hydrogenous Os_i values, we analyzed ten samples from the Qingshankou
156 Formation on a Thermo Scientific Triton thermal ionization mass spectrometer at Durham
157 University via the established procedures of Selby and Creaser (2003) (see Appendix). We
158 selected samples in Member 1 and lowermost Members 2 and 3 from horizons proposed to
159 record biomarker evidence for marine incursions (Hu et al., 2015). Additionally, we analyzed
160 samples from the Turonian-aged black shales of Site 1259 at Demerara Rise (Tropical North
161 Atlantic ODP Leg 207) and Coniacian OAE3 interval in the Angus Core from the WIB. We
162 present these sample sets to characterize open and epicontinental marine Os_i values, respectively,
163 for comparison with the coeval Qingshankou Formation record and to test the hypothesis of
164 marine incursions into the Songliao Basin. To correct for post-depositional ^{187}Re decay to ^{187}Os
165 (see Appendix), we assign numerical ages to samples using an age model at Demerara Rise
166 (updated from Bornemann et al., 2008) and the existing Angus Core (Joo and Sageman, 2014)
167 and SK1-S age models (Sect. 3.1).

168 **4. Results**

169 4.1 Bulk carbon chemistry TOC, C/N trends

170 Weight percent TOC decreases upcore within the Qingshankou Formation from
171 maximum values in the laminated Member 1, consistently above 2% and up to ~8% TOC, to
172 values in Members 2 and 3 that rarely exceed 1% TOC. In TOC-rich Member 1, C/N ratios are
173 elevated ($C/N = 8.5-25.6$) above typical lacustrine algal values ($C/N < 8$; Meyers, 1994) (Fig. 2;
174 see Table A.1). Occasionally, discrete horizons in Members 2 and 3 record elevated TOC spikes
175 punctuating the background pattern of decaying TOC levels. These horizons are accompanied
176 by increased C/N and enriched $\delta^{13}C_{org}$, with C/N ($C/N = 15-25$) approaching land-based vascular

177 plant organic matter values (C/N>25; Meyers, 1994) above the background lacustrine algal
178 organic matter values. Additionally, new percent carbonate values are low, yet detectable
179 throughout the studied interval (median=6.9%, max=22.5%) from scattered ostracods
180 (Chamberlain et al., 2013; Wan et al., 2013).

181 4.2 Carbon isotopes

182 Bulk organic carbon isotope values in the studied interval are highly variable (-24 to -
183 32.5‰) (Fig. 2; Table A.1-2). Some of this variability corresponds to changing facies, such as
184 comparatively enriched $\delta^{13}\text{C}_{\text{org}}$ in fluvial facies of the Quantou and Yaojia Formations (generally
185 $\delta^{13}\text{C}_{\text{org}} > -27\text{‰}$). However, lacustrine $\delta^{13}\text{C}_{\text{org}}$ values are also highly variable. Samples from
186 Qingshankou Member 1 are strongly depleted in bulk $\delta^{13}\text{C}_{\text{org}}$, with an average value of -30.61‰
187 ($1\sigma \text{SD} = \pm 1.33\text{‰}$) and minimum of -32.4‰. Interestingly, the bulk $\delta^{13}\text{C}_{\text{org}}$ of Member 1 is more
188 depleted than both average Cretaceous marine (-27 to -29‰) and terrestrial (-24 to -25‰) end
189 members (Arthur et al., 1985). The $\delta^{13}\text{C}_{\text{org}}$ values of Members 2 and 3 are more enriched
190 (median = -28.7‰). However, this interval preserves high $\delta^{13}\text{C}_{\text{org}}$ variability ($1\sigma \text{SD} = \pm 1.5\text{‰}$). A
191 sustained positive carbon isotope excursion (+3.0 to +4.5‰) is noted in Members 2 and 3 (1380-
192 1440 m) corresponding closely to the timing of OAE3 as recorded by a +1‰ CIE in the WIB
193 (Joo and Sageman, 2014). Smoothed $\Delta^{13}\text{C}$ in SK1-S decreases up-core from the base of Member
194 1 from ~36‰ to ~31‰, and further decreases by ~3‰ through OAE3. In the Angus Core
195 (WIB), smoothed $\Delta^{13}\text{C}$ records a similar but lower magnitude decrease (~-0.5‰) through OAE3.
196 In that interval, $\delta^{13}\text{C}_{\text{carb}}$ is relatively stable ($1\sigma \text{SD} = \pm 0.19\text{‰}$) with average $\delta^{13}\text{C}_{\text{carb}}$ values
197 (+1.84‰) comparable to coeval values in the English Chalk reference curve (Jarvis et al., 2006).

198 4.3 XRF data

199 Given that facies changes can significantly alter elemental chemistry of sediments, we
200 limit discussion and interpretation of XRF data to the lacustrine facies of the Qingshankou
201 Formation. Redox sensitive trace elements that accumulate in low oxygen conditions, such as
202 Co, Cr, Ni, Pb, V, and Cu, show subtle to significant enrichment in the TOC-rich Qingshankou
203 Member 1, whereas Mn, which remobilizes in anoxic environments, shows decreased
204 concentrations (Table A.2). The V+Cr concentrations, a trace element proxy for nitrate
205 reduction and low O₂ (Sageman et al., 2014a), are significantly enriched in Member 1 (>200
206 ppm) above background values for the Qingshankou Formation (~150 ppm) (Fig. 3). Copper
207 concentrations spike at 1770 m and are strongly positively correlated with TOC ($r^2 = 0.87$) and
208 C/N ($r^2 = 0.73$) in Member 1 (n=7).

209 Several trace elements and elemental ratios serve as proxies for water column euxinia
210 where free hydrogen sulfide, a product of sulfate reduction, is present (Fig. 3) (Tribovillard et al.,
211 2006). The V/(V+Ni) values, a proxy for anoxia and euxinia (Hatch and Leventhal, 1992),
212 average 0.68-0.74 in the Qingshankou Formation with enrichments in Member 1 (0.74-0.77).
213 Throughout the Qingshankou Formation the V/(V+Ni) ratios fall consistently into the non-
214 sulfidic anoxic range. The concentrations of Mo, one of the most robust elemental indicators of
215 euxinia, average 8 ppm (1σ SD±5 ppm, max [Mo] = 21.7 ppm) and show no notable increase in
216 Qingshankou Member 1. Ratios of Mo/Al average 0.78×10^{-4} (1σ SD± 0.48×10^{-4}) exceed average
217 shale values (0.32×10^{-4} , Wedepohl, 1971) throughout most of the Qingshankou, suggesting
218 authigenic enrichment. However, Mo/TOC is poorly correlated ($r^2 = 0.19$) and reaches a
219 minimum in the TOC-rich Member 1. Despite high TOC, the S/Fe and Fe/Al ratios, which are
220 known to increase with authigenic pyrite formation, do not increase in Member 1 (Fig.3). Also,
221 we calculate the chemical index of alteration (CIA), which is a proxy for weathering intensity

222 (Table A.2; Fig. 3) (Nesbitt and Young, 1982). The carbonate corrected CIA is relatively stable
223 throughout the Qingshankou Formation, although it does preserve a ~10% decrease during the
224 OAE3 CIE, typically indicative of decreased weathering intensity.

225 4.4 Initial osmium isotope ratios

226 The Os_i from the Qingshankou Formation range between 0.66 and 0.96 (Figs. 2 & 6).
227 Osmium concentrations are similar through the interval (^{192}Os conc. = 7-17 ppt; Table A.1).
228 Rhenium concentrations are generally higher in Qingshankou Member 1 (avg. Re conc. = 3.80
229 ppb, 1σ SD \pm 0.18 ppb) than in Members 2 and 3 (avg. Re conc. = 1.99 ppb, 1σ SD \pm 1.66 ppb),
230 except for one point at 1325 m (Table A.1). The Os_i values are the most radiogenic through the
231 TOC-rich mudstones in the Member 1 (avg. Os_i = 0.90, 1σ SD \pm 0.05) (Fig. 6). In the lowermost
232 Members 2 and 3, one sample at ~1685 m yields a slightly less radiogenic value (Os_i = 0.76)
233 compared to the samples below (Os_i = 0.87) and above (Os_i = 0.91). Relatively stable (Os_i range
234 = 0.11) Os_i values from the upper sample set in Qingshankou Members 2 and 3 characterize the
235 SK1-S interval spanning OAE3. The Os_i values in this interval are slightly less radiogenic (avg.
236 Os_i = 0.72) than in Qingshankou Member 1.

237 A time correlative open marine section from ODP Site 1259 at Demerara Rise, yields
238 samples highly enriched in osmium (^{192}Os conc. = 31-366 ppt) and highly variable in rhenium
239 concentrations (Re conc. range = 12-142 ppb) (Table A.1.1). The Os_i values are more
240 unradiogenic than values recorded in the Songliao Basin and are relatively stable over
241 approximately 3 Ma, ranging between 0.55 and 0.71 (avg. Os_i = 0.61, 1σ SD \pm 0.06) (Figs. 2 & 6;
242 Table A.1.1). The Os_i samples from the marine WIB spanning OAE3 preserve no prominent
243 excursion through the event (Os_i = 0.54-0.58) and are highly enriched in osmium (^{192}Os conc. =
244 136-260 ppt) and rhenium (Re conc. = 191-361 ppb).

245 5. Interpretation

246 5.1 Qingshankou Formation $\delta^{13}\text{C}_{\text{org}}$ chemostratigraphy and OAE3

247 Carbon isotope excursions have proven utility as isochronous horizons to correlate
248 stratigraphic records globally (Jarvis et al., 2006; Wendler, 2013). However, a host of factors in
249 a given sedimentary basin can alter bulk organic carbon isotopic ratios ($\delta^{13}\text{C}_{\text{org}}$) in addition to
250 changes in the global carbon cycle, such as changing organic matter type and metabolic
251 pathways. Our comparison of Gaussian kernel smoothed $\delta^{13}\text{C}_{\text{org}}$ records from the Songliao
252 Basin and WIB (Joo and Sageman, 2014) demonstrates one negative CIE, possibly the
253 Bridgwick Event (Jarvis et al., 2006), and one positive CIE, OAE3 (also referred to as the
254 Whitefall/Kingsdown CIEs), which broadly correspond in age and duration (Fig. 4). Despite
255 similar CIE durations, we detect an offset of 330 ka after cross-correlation of the two basins'
256 anchored $\delta^{13}\text{C}_{\text{org}}$ time series, with ages of the Songliao Basin CIEs being older than ages of the
257 WIB CIEs (see Fig. A.1). This offset could arise from the presence of “reworked and/or detrital
258 zircon” in radioisotopically dated samples of SK1-S (Wang et al., 2016b), or undetected Upper
259 Turonian/Lower Coniacian hiatuses in SK1-S or the WIB (Sageman et al., 2014b). Although
260 partially offset in age, we note that these CIEs overlap within temporal uncertainty of time scales
261 in the Songliao Basin (± 181 ka, Sect. 3.1) and in the WIB (e.g., Turonian/Coniacian Boundary =
262 ± 380 ka; Sageman et al., 2014b). Moreover, the similarity in the timing and duration of CIEs
263 signifies agreement between East Asian and North American time scales, validating
264 intercontinental comparison of geologic datasets (e.g., paleoclimatic, paleobiologic). We note
265 that the CIEs are amplified in the lacustrine Songliao Basin (+3.0 to +4.5‰) compared to the
266 marine WIB ($\sim +1\%$) (Joo and Sageman, 2014) and other marine $\delta^{13}\text{C}_{\text{carb}}$ records in the WIB
267 (Tessin et al., 2015; this study) and elsewhere (Wagreich, 2012; Wendler, 2013, and references
268 therein).

269 The identification of OAE3 within a lake system in the terrestrial Qingshankou Members 2
270 and 3 permits comparisons to marine records of the event aided by a highly resolved temporal
271 framework. The lowest TOC levels in the Qingshankou Formation in SK1-S occur during OAE3
272 (Fig. 2). This is also the case for OAE2, since the event is preserved in the TOC-lean Quantou
273 Formation in SK1-S (Chamberlain et al., 2013). Accordingly, we confirm that OAEs do not
274 necessarily correspond to lake anoxic events in East Asian lake systems (Wu et al., 2013), and
275 that these lakes were not significant organic carbon depocenters during OAEs. We infer that
276 during OAE3, reduced primary productivity and/or enhanced bottom-water oxygenation through
277 regular lake overturning, in response to climatic forcing, played a role in decreasing organic
278 carbon preservation.

279 In both SK1-S and the WIB, $\delta^{13}\text{C}_{\text{org}}$ enrichment and a diminutive excursion in $\delta^{13}\text{C}_{\text{carb}}$ (Fig.
280 2) (ostracod - Chamberlain et al., 2013) across OAE3 controls a decrease in $\Delta^{13}\text{C}$ (Fig. 5). In
281 SK1-S, this $\delta^{13}\text{C}_{\text{org}}$ excursion is not likely due to changing organic matter source given
282 consistently low C/N. Another coeval $\Delta^{13}\text{C}$ record from the Portland Core (Colorado) in the
283 WIB with variable organic matter type has been interpreted as diagenetically altered (Tessin et
284 al., 2015). However, there is little evidence for $\delta^{13}\text{C}_{\text{org}}$ or $\delta^{13}\text{C}_{\text{carb}}$ diagenesis in the Angus Core
285 in the OAE3 interval (Appendix). Therefore, we attribute the OAE3 $\delta^{13}\text{C}_{\text{org}}$ excursion and
286 decreased $\Delta^{13}\text{C}$ to diminished fractionation between dissolved inorganic carbon and
287 photosynthate, driven by decreased dissolved CO_2 levels (Kump and Arthur, 1999). In the
288 marine record, this is consistent with atmospheric pCO_2 drawdown commensurate with organic
289 carbon sequestration in marine shales globally, as has been inferred for OAE2 (e.g., Jarvis et al.,
290 2011).

291 However, lacustrine pCO₂ proxies (i.e., $\Delta^{13}\text{C}$) cannot be interpreted as direct records of
292 atmospheric pCO₂ since modern large lakes analogous to the depositional environment of the
293 Qingshankou Formation are net sources of CO₂ to the atmosphere, such as the East African rift
294 lakes (Alin and Johnson, 2007). Over longer time periods, riverine inputs of dissolved CO₂ are
295 the primary control on modern lacustrine CO₂ levels in mid-latitude lakes, and vary as a function
296 of soil pCO₂ and catchment productivity (Maberly et al., 2013). The sedimentary geochemistry
297 of modern and Lower Cretaceous rift lakes in Africa record these landscape processes as well
298 (Harris et al., 2004; Talbot et al., 2006), since dissolved CO₂ levels exert a significant control on
299 carbon isotope fractionation in lakes (Hollander and Smith, 2001). During OAE3, the Songliao
300 lake system preserves a comparatively larger shift in $\delta^{13}\text{C}_{\text{org}}$ and $\Delta^{13}\text{C}$ than the WIB (Fig. 5). We
301 attribute this to a greater decrease in dissolved CO₂ in the Songliao lake system, driven by
302 reduced soil productivity in the basin's catchment through OAE3. This is consistent with a
303 scenario of atmospheric pCO₂ drawdown and cooling reflected in decreased marine $\Delta^{13}\text{C}$ in the
304 WIB.

305 Compared to OAE2, pCO₂ drawdown through OAE3 is interesting since the event is not
306 represented by a discrete archetypal black shale or anoxic/euxinic interval (Wagreich, 2012;
307 Lowery et al., 2017) and preserves a relatively diminished marine CIE (Jarvis et al., 2006;
308 Locklair et al., 2011; Joo and Sageman, 2014). One mechanism for sustaining an OAE invokes
309 enhanced weathering of continentally derived nutrients (e.g., P), following volcanic CO₂ pulses
310 from large igneous province (LIPs) emplacement (cf. Jenkyns, 2010). However, marine Os_i
311 values spanning OAE3 in the WIB do not record evidence for submarine LIP volcanism (i.e.,
312 unradiogenic Os_i shift) (Fig. 6; Sect. 5.3), as is the case for OAE2 (Turgeon and Creaser, 2008;
313 Du Vivier et al., 2014); nor do they record evidence for accelerated global continental

314 weathering rates (i.e., a shift to more radiogenic Os_i). Likewise, weathering proxies from the
315 Songliao Basin's OAE3 interval are either stable, such as Os_i (Figs. 2 & 6), or suggest a decrease
316 in weathering intensity, such as $\Delta^{13}\text{C}$ (Fig. 4) and CIA (Fig. 3). Although we caution that these
317 local observations are of a relatively minor OAE and cannot be assumed globally representative,
318 these results suggest that the perturbations to the Earth system that triggered and sustained OAE3
319 are unique from those that triggered more severe OAEs (e.g., OAE2, Toarcian OAE).

320 Overall, the Qingshankou Formation $\delta^{13}\text{C}_{\text{org}}$ chemostratigraphy is highly variable through
321 Member 1 and the lowermost Members 2 and 3. This suggests that dynamic local
322 biogeochemical cycling and environmental conditions, in addition to the global carbon cycle,
323 affected the $\delta^{13}\text{C}_{\text{org}}$ values in this interval (Fig. 2). Furthermore, we interpret the combination of
324 highly depleted $\delta^{13}\text{C}_{\text{org}}$ values (-32.4‰ minimum), high C/N typical of nitrogen-poor anoxic
325 bottom-waters (Meyers, 1994), and redox-sensitive XRF data (Sect 5.2), as evidence that
326 methanogenesis and methanotrophy (Hollander and Smith, 2001) influenced bulk $\delta^{13}\text{C}_{\text{org}}$ values
327 in the TOC-rich Qingshankou Member 1. Extremely $\delta^{13}\text{C}$ depleted methyl hopane compounds (-
328 42 to -50‰) in Member 1 equivalent oil shales from the Ngn-02 Core (Bechtel et al., 2012)
329 confirm the role of methanotrophy in the unit. As a result, we cannot solely attribute the
330 depleted $\delta^{13}\text{C}_{\text{org}}$ in Member 1 to the global Bridgwick CIE, and instead we interpret this interval
331 as at least partially recording burial of lacustrine methanotrophic biomass. Increased dissolved
332 CO_2 in the lake from increased catchment productivity may have also contributed to the
333 amplified negative CIE in Member 1 (Hu et al., 2015).

334 5.2 Low sulfate and redox conditions in lacustrine Qingshankou Formation

335 The redox sensitive trace element dataset from Qingshankou Member 1 (Sect. 4.3) provides a
336 record of non-euxinic anoxic bottom-waters during deposition. Consistent trends among a

337 variety of the evaluated trace element proxies lend confidence to the paleo-redox reconstructions.
338 Combined, low Mn (<400 ppm), elevated V+Cr (>200 ppm) and (V+Cr)/Al, and elevated
339 V/(V+Ni) (>0.7, Hatch and Leventhal, 1992) in Member 1 indicate anoxia (Fig. 3).

340 Compared to the marine realm, biogeochemical cycling in anoxic lakes typically operates
341 with fundamentally different dominant microbial pathways (e.g., methanogenesis and
342 methanotrophy), since lakes generally have much lower concentrations of dissolved sulfate and
343 redox-sensitive trace elements such as molybdenum. Microbial sulfate reduction (MSR) in
344 anoxic low sulfate lakes tends to draw down the sulfate reservoir and limit sulfur isotope
345 fractionation leaving pyrite isotopic values enriched (Gomes and Hurtgen, 2013). In
346 Qingshankou Member 1, $\delta^{34}\text{S}_{\text{pyrite}}$ is highly enriched (+15 to +20‰) (Fig. 3) (Huang et al., 2013).
347 Huang et al. (2013) attributed this to a complex disproportionation and transport model
348 dependent on isotopic heterogeneity within the basin. However, considering our new trace
349 element data, we propose an alternative interpretation, namely that the enriched $\delta^{34}\text{S}_{\text{pyr}}$ values
350 were consequences of inhibited MSR fractionation related to low sulfate concentrations under
351 non-marine depositional conditions. This phenomenon is noted in Holocene non-marine Black
352 Sea mudstones (>~8 ka) deposited during basin isolation from the global ocean (Calvert et al.,
353 1996). In another test of sulfate levels and seawater connectivity, TOC/S ratios are generally
354 <2.8 in marine sediments (Bernier, 1982), although some lacustrine mudstone values fall below
355 this threshold (e.g., Calvert et al., 1996). In Qingshankou Member 1, TOC/S ratios all exceed
356 this threshold (average TOC/S = 14; this study) and are consistent with pyrite burial limited by
357 low sulfate levels (Bechtel et al., 2012). Concentrations of molybdenum (average = 8 ppm),
358 another robust proxy for the presence of free sulfide, remain below minimum thresholds
359 established for euxinic mudstones (25 ppm Mo-depleted waters, 65 ppm Mo-replete waters,

360 Scott and Lyons, 2012), but molybdenum concentrations and Mo/Al values do exceed average
361 shale values (2.6 ppm and 0.32×10^{-4} respectively, Wedepohl, 1971), suggesting MSR was active,
362 but limited by low sulfate and molybdate concentrations in the lake (Fig. 3). In Mo-replete
363 marine waters, sedimentary Mo concentrations positively correlate with TOC (Algeo and Lyons,
364 2006). However, this relationship is not observed in the Qingshankou Formation ($r^2 = 0.19$) and
365 Mo/TOC ratios are lowest in the TOC-rich Member 1 (Fig. 3) (Sect. 4.3). Influxes of sulfate and
366 molybdenum-replete marine water would have elevated MSR and corresponding pyrite burial,
367 leading to increases in Fe/Al, Mo/TOC, and S concentrations. Our proxy results from SK1-S do
368 not record such shifts, and we therefore infer that low sulfate non-marine conditions prevailed
369 throughout deposition of the Qingshankou Formation.

370 Depleted bulk $\delta^{13}\text{C}_{\text{org}}$ (*this study*; Hu et al., 2015) and methyl hopane $\delta^{13}\text{C}$ values (Bechtel et
371 al., 2012) reinforce the hypothesis that sulfate reduction was limited and that methanogenic and
372 methanotrophic microbial metabolisms were prevalent during deposition of Qingshankou
373 Member 1 (Sect. 5.1). Additionally, concentrations of certain trace elements, such as Cu, Ni, Co,
374 that play central roles in enzymes facilitating methanogenesis and methanotrophy (Glass and
375 Orphan, 2012), spike in Member 1. This may indicate enhanced methanogenesis and
376 methanotrophy in the anoxic lacustrine mudstones (Fig. 3). Alternatively, it could reflect that
377 metals are complexed with organic matter independent of methanotrophic activity in Member 1
378 (TOC and Cu covariance: $r^2 = 0.88$). Regardless, proxies such as elemental concentrations,
379 methanotrophic biomarkers, sulfur isotopes, laminated mudstones, and bulk $\delta^{13}\text{C}_{\text{org}}$, consistently
380 indicate persistent anoxia and methanogenesis in low sulfate waters (i.e., MSR inhibited) during
381 deposition of the TOC-rich Qingshankou Member 1.

382 5.3 Seawater incursion hypothesis and Os_i chemostratigraphy

383 Incursions of dense marine water into the Songliao Basin during sea level highstands
384 have been invoked as a mechanism to stratify the basin's water column, intensifying bottom-
385 water anoxia, and ultimately driving deposition of Member 1's TOC-rich source rocks (Hou et
386 al., 2000; Huang et al., 2013; Hu et al., 2015). Mixing of marine and lacustrine water bodies,
387 each with distinct chemical properties, would perturb the chemostratigraphic record, including
388 Os_i values. However, our Os_i chemostratigraphy from SK1-S preserves no compelling evidence
389 for marine incursions in TOC-rich intervals. Instead, the Os_i data in Member 1 are consistently
390 the most radiogenic values of SK1-S (Fig. 6). We conclude that this observation is inconsistent
391 with incursions of less radiogenic open marine osmium as measured at Demerara Rise, and
392 resembles the more radiogenic Os_i records existing from lacustrine mudstones elsewhere (Poirier
393 and Hillaire-Marcel, 2011; Cumming et al., 2012; Xu et al., 2017). At Demerara Rise, an
394 average open marine Os_i of ~0.6 for mid-Turonian to Coniacian samples is considered to be the
395 best estimate of the steady-state open marine value for the Late Cretaceous governed by plate
396 tectonic configurations (i.e., long-term average continental weathering and hydrothermal fluxes)
397 given similar results from comparably aged marine records, such as post-OAE2 (Du Vivier et al.,
398 2014) and our new WIB OAE3 data (Fig. 6). However, we note that the WIB Os_i data is likely
399 more radiogenic than open marine Os_i , due to the marine basin's epicontinental setting and
400 mixing with continentally derived osmium.

401 One Os_i data point (1685 m) in the lower Songliao Os_i sample set is less radiogenic than
402 other nearby horizons. This is also an interval where concentrations of 24-n-
403 isopropylcholestane spike (biomarker typically attributed to marine organisms, Hu et al., 2015)
404 and XRF sulfur concentrations more than double for one data point. It is possible that this
405 horizon indicates a minor seawater incursion. However, we consider that this is unlikely since

406 the horizon is not associated with any spikes in euxinic-sensitive trace elements (e.g., Mo,
407 V/V+Ni, Sect. 5.2) (Fig. 3), TOC enrichments, or changes in lithology, and due to additional
408 paleogeographic factors discussed below.

409 Our trace element and Os_i evidence contrary to a Songliao Basin-marine connection
410 during deposition of Qingshankou Member 1 is consistent with many lines of previous
411 observation such as: a lack of foraminifera, calcareous nannofossil, or marine macrofossil
412 preservation in the Qingshankou Formation of SK1-S (Wan et al., 2013; Xi et al., 2016), non-
413 marine phytoplankton (Zhao et al., 2014), depleted non-marine $\delta^{18}\text{O}$ values (Chamberlain et al.,
414 2013), plate tectonic reconstructions placing the nearest marine body at least 500 km away, and
415 evidence for coastal mountain building between the Songliao Basin and Pacific Ocean (Yang,
416 2013) (Fig.1). Contrastingly, observations of $\delta^{34}\text{S}_{\text{pyr}}$ (Huang et al., 2013) and biomarkers (C30
417 steranes e.g., 24-isopropylcholestane, Hu et al., 2015) have been interpreted as evidence for
418 marine incursions. Additionally, a few poorly preserved foraminifera have been reported in
419 Member 1 elsewhere in the basin (Xi et al., 2016), although no photographs or depths of
420 occurrence are accessible to our knowledge, precluding verification, taxonomic identification,
421 and correlation to horizons in the SK1-S core. It is possible to reconcile our geochemical
422 datasets with enriched $\delta^{34}\text{S}_{\text{pyr}}$ data in Member 1 if a low sulfate lake water column inhibited
423 sulfur isotope fractionation (Sect. 5.2). Explaining the presence of 24-n-isopropylcholestane
424 without invoking seawater incursions is more challenging, because the biomarker has been
425 classified as an indicator of marine organic matter (Moldowan et al., 1990). However, we note
426 that C30 steranes, including molecular precursors to 24-isopropylcholestane, have been detected
427 in a modern French lake (Wunsche et al., 1987). If the biomarkers previously reported from the
428 Songliao Basin (Hu et al., 2015) are instead derived from non-marine dinoflagellates, sponges or

429 microbial symbionts producing C30 sterols, are detritally re-worked, or are the molecular
430 diagenetic products of organic matter degradation in a thermally mature interval of the basin (cf.
431 Feng et al., 2010), then their occurrences would be consistent with our interpretation of the Os_i
432 record as that of an isolated lacustrine basin.

433 Alternatively, our Os_i record from the Songliao Basin could have been dominated by a
434 high flux of continentally derived radiogenic Os_i from nearby catchments, masking a record of
435 seawater incursions via mixing. A recent study of Holocene Os_i profiles in a transect off
436 Greenland's coast demonstrated that Os_i records can be sensitive to local fluxes of weathered
437 osmium (Rooney et al., 2016). However, we consider that this masking scenario is less likely in
438 the Songliao Basin, since Members 2 and 3 lack evidence for marine incursions, but do not show
439 evidence for extremely radiogenic Os_i values within the weathered catchments (Fig. 6).
440 Additionally, two strontium isotope measurements in the lower Qingshankou Formation (avg.
441 $^{87}\text{Sr}/^{86}\text{Sr} = 0.70767$, $1\sigma \text{SD} \pm 0.00005$) are not extremely radiogenic, but are offset from coeval
442 marine ratios (Chamberlain et al., 2013). Their values do not preserve evidence for marine
443 incursions, nor do they indicate weathering of extremely radiogenic lithologies within the basin's
444 catchment. This suggests that Os_i chemostratigraphy could resolve evidence of marine
445 incursions if present. We note that it is possible that a brief marine incursion occurred in an
446 unsampled interval, as temporal resolution of Os_i samples range from 100-300 ka in Member 1.
447 However, we selected samples from horizons with published proposed evidence (i.e., biomarker)
448 for marine incursions (Fig. 6). Additionally, we observe no abrupt lithologic alterations in SK1-
449 S commonly associated with lacustrine-marine transitions in other basins (Calvert et al., 1996;
450 Poirier and Hillaire-Marcel, 2011 and references therein).

451 In the younger OAE3 interval of Qingshankou Members 2 and 3, the Os_i data are less
452 radiogenic, and approach values from the epicontinental marine WIB (Fig. 6). Again, we do not
453 interpret these data as evidence for a prolonged marine connection to the Songliao Basin,
454 because little evidence exists of marine microfossils (Xi et al., 2016) or sulfate replete waters
455 (Sect. 5.2; Fig. 3) in this interval. Instead, we attribute the lower Os_i values in Qingshankou
456 Members 2 and 3 to the weathering of the near contemporaneous mid-Coniacian flood basalts
457 within the Songliao Basin (Wang et al., 2016a), which would possess mantle-like $^{187}Os/^{188}Os$
458 compositions (~ 0.13) mixing with lake waters (Fig. 6). We also note that Os_i values are
459 relatively stable through OAE3, suggesting muted changes in the weathering flux of osmium
460 (Sect. 5.1).

461 5.4 Qingshankou Formation Depositional Model

462 Given limited evidence for incursions of saline marine waters in Member 1 (Sect. 5.2-
463 5.3), we propose alternative mechanisms for lake stratification that could be responsible for
464 enhanced anoxia (Sect. 5.1-5.2) and resulting enhanced organic matter burial. Based on modern
465 and paleo analogs, we outline a new conceptual model characterizing bottom-water redox,
466 biogeochemical cycling, and physical processes (stratification, mixing) for the lacustrine
467 Songliao rift basin through the Qingshankou Formation interval (Fig. 7). Sustained stratification
468 of large meromictic lakes is critical in generating TOC-rich mudstone deposits, as settling
469 organic matter from highly productive lacustrine surface waters is remineralized passing through
470 isolated and progressively deoxygenated bottom-waters (Demaison and Moore, 1980). For any
471 scenario of bottom-water anoxia, the depth of the stratified lake would need to exceed the wave-
472 base mixing depth. This considerable minimum depth (e.g., ~ 100 m) on a large paleolake with
473 an expansive fetch (~ 200 - 300 km) for generating waves, supports the assertion that the lake was

474 deeper and more expansive during Member 1 than Members 2-3 (Feng et al., 2010), favoring
475 meromixis within a deep lake.

476 Water column density stratification likely arose in Qingshankou Member 1 from
477 gradients in temperature, salinity, temperature, and/or dissolved gases from organic matter
478 remineralization (e.g., Boehrer and Schultze, 2008), inhibiting lake overturning and
479 reoxygenation of bottom-waters (Fig. 7). In the case of thermal stratification, most modern
480 meromictic lakes do not occur outside the tropics (e.g., Lake Tanganyika), and are reinforced by
481 additional density gradients. However, the mid-Cretaceous was a period of extreme greenhouse
482 warmth. Intervals of high temperature and low seasonality (i.e., obliquity minima) would have
483 inhibited the Songliao Basin water column overturning and reduced dissolved oxygen levels, and
484 indeed palynological datasets indicate a semi-humid subtropical climate during deposition of
485 Member 1 (Wang et al., 2013; Zhao et al., 2014). Although additional paleoclimate data are
486 necessary to fully test this hypothesis, our idea that elevated temperatures would have inhibited
487 lake overturning is consistent with general reconstructions for the warm mid-Cretaceous. Even
488 though we do not detect seawater incursions in this study and no evaporites are associated with
489 Member 1, evidence for elevated salinity is inferred from paleontological investigations that
490 have documented slightly brackish algae, dinoflagellate, and ostracod assemblages (Zhao et al.,
491 2014; Xi et al., 2016). Organic geochemical investigations have also detected salinity biomarkers
492 (e.g., gammacerane, β -carotane) in Member 1 (Bechtel et al., 2012). Several ostracod $\delta^{18}\text{O}$ and
493 $\delta^{13}\text{C}_{\text{carb}}$ values are enriched in Member 1 and lowermost Members 2 and 3 compared to
494 overlying samples (Chamberlain et al., 2013), possibly related to enhanced evaporation rates and
495 consistent with dolomite laminae preservation in the interval (Talbot, 1990; Gao et al., 2009;
496 Wang et al., 2009). Further, authors interpret covariation between $\delta^{18}\text{O}$, $\delta^{13}\text{C}_{\text{carb}}$, Mg/Ca, and

497 Sr/Ca as evidence for closed basin conditions throughout the Qingshankou Formation, signifying
498 a lake basin sensitive to changing precipitation to evaporation (P/E) rates (Chamberlain et al.,
499 2013). On the other hand, palynology suggests the climate was semi-humid during Member 1
500 (Wang et al., 2013) which would have limited evaporation and salinity's role in density
501 stratification, although others report that diagenesis possibly biased palynological reconstructions
502 (Zhao et al., 2014). A final process that we suspect contributed to elevated bottom-water density
503 in Lake Songliao is the addition of dissolved biochemical products (e.g., HCO_3^- , H_2S , CH_4 , etc.)
504 from remineralization of organic matter (Fig. 7a). Evidence for methanogenesis, as well as
505 heterotrophic biomarkers (e.g., hopanoids) (Bechtel et al., 2012), indicate microbial reworking of
506 biomass in Member 1. This is consistent with increased bottom-water density via "biogenic
507 meromixis", stratification from dissolved biochemical products (Boehrer and Schultze, 2008).
508 Our combined model for Lake Songliao's stratification draws on many physical and geochemical
509 processes, such as temperature gradients, biogenic meromixis, and elevated salinity. We
510 hypothesize that these processes were controlled both by tectonic (i.e., lake depth) and climatic
511 (e.g., P/E) conditions that contributed to a stagnant pool of anoxic bottom-water conducive to
512 deposition of TOC-rich mudstones.

513 Conversely in Members 2 and 3, we propose that TOC-lean grey mudstones were the
514 result of enhanced water column overturning and improved oxygenation of lake bottom-waters.
515 During OAE3, the interval of lowest TOC in the Qingshankou Formation, factors such as,
516 increased seasonality, freshening of bottom-waters, more vigorous wave mixing (i.e., higher
517 surface wind velocity), and/or lake shallowing likely contributed to bottom-water reoxygenation
518 and the demise of stratification (Fig. 7b).

519 **6. Conclusions**

520 Through geochemical analyses, we reconstruct local Late Cretaceous paleoclimate records
521 and lacustrine carbon burial dynamics of the Qingshankou Formation in the Songliao Basin of
522 northeast China. Correlation of Turonian-Coniacian $\delta^{13}\text{C}_{\text{org}}$ records from the Songliao Basin to
523 the WIB confirms the presence of OAE3 in a low-TOC interval of Qingshankou Members 2 and
524 3, providing a unique record OAE3 in a lake system. The chemostratigraphic results from the
525 Songliao Basin demonstrate that OAE2 and OAE3 did not trigger elevated organic carbon burial
526 in an expansive East Asian lake. Furthermore, we attribute significant decreases in marine and
527 lacustrine $\Delta^{13}\text{C}$ to a drawdown of pCO_2 and cooling through OAE3 and decreased soil
528 productivity in the Songliao catchment. This finding is consistent with enhanced burial of
529 organic carbon on a global scale and is analogous to interpretations for other prominent
530 Cretaceous OAEs (Arthur et al., 1988; Barclay et al., 2010; Jarvis et al., 2011). However, Os_i
531 stratigraphy records no evidence for significant changes in global volcanism though OAE3,
532 which suggests an event trigger unique from OAE2 (i.e., LIP volcanism). We encourage future
533 investigations, employing, for example, compound specific $\delta^{13}\text{C}$ chemostratigraphy and high-
534 resolution paleoclimate proxies, to further resolve the robustness of $\delta^{13}\text{C}$ correlations and better
535 elucidate the paleoclimatic response of the Songliao basin lacustrine units to OAE3.

536 Radiogenic Os_i values recorded through the TOC-rich Qingshankou Member 1 indicate that
537 enhanced organic carbon burial and source rock formation occurred in a lacustrine basin isolated
538 from the global ocean. Although our Os_i sample resolution is limited and marine incursions
539 could have alluded detection in this initial survey, our higher resolution redox sensitive trace
540 element data, as well as most existing paleogeographic, chemostratigraphic, and paleobiologic
541 data, are also consistent with mudstone deposition in a low sulfate, lacustrine setting through
542 Member 1. Our synthesis of existing stratigraphic datasets into a source rock depositional model

543 for Qingshankou Member 1 outlines lacustrine stratification and biogeochemical cycling
544 scenarios independent of marine incursions. This study underscores the potential to reconstruct
545 Late Cretaceous paleoclimate, lake system responses to OAEs, and terrestrial carbon burial
546 dynamics from lacustrine mudstones archives, such as those found in the Songliao Basin.

547 Acknowledgements

548 We thank Professor Chengshan Wang (China University of Geosciences, Beijing) for facilitating
549 sampling of the SK1-S core. This research also benefited greatly from the assistance of
550 Northwestern University lab managers Grace Schellinger and Dr. Koushik Dutta, and research
551 assistant Katarina Savatic during measurement of carbon chemistry; Antonia Hofmann and Dr.
552 Joanna Hesselink of Durham University with rhenium-osmium isotope analyses; and Juan
553 Lezama-Pacheco and Danielle Moragne at Stanford University with XRF analyses. We thank
554 three anonymous reviewers who provided valuable feedback and improved the quality of the
555 manuscript. U.S. National Science Foundation grant funding was provided to B.B.S. (EAR-
556 1424474), and to C.P.C. and S.A.G. (EAR-1423967). National Basic Research Program of
557 China funding was provided to Y.G. (2012CB8220000). D.S. acknowledges the TOTAL
558 Endowment Fund.

559

560 Appendix A. Supplementary material

561 Supplementary material for this article can be found online at (link)

562

563 **Figure Captions**

564 **Fig. 1: a.)** Palinspastic map of East Asia during the Coniacian-E. Campanian, including the
565 studied Songliao Basin and surrounding physical geographic and plate tectonic features
566 (SYB=Subei-Yellow Sea Basin; modified from Yang, 2013). **b.)** Map of SK1-S core and facies
567 during deposition of Qingshankou Member 1 (modified from Feng et al., 2010). **c.)** Cross section
568 A-A' from Wang et al. (2013) depicting Cretaceous lithostratigraphic units of the Songliao Basin
569 including the Qingshankou Formation (dark blue).

570 **Fig. 2:** Chemostratigraphic record from SK1-S core spanning the upper Quantou through the
571 Yaojia formations. Stratigraphic column modified from Wu et al. (2013). Red stars represent
572 bentonite horizons with CA-ID-TIMS U/Pb zircon ages (Wang et al., 2016). Hiatus at the
573 Qingshankou/Yaojia contact identified by Feng et al. (2010). The $\delta^{13}\text{C}_{\text{carb}}$ (red) data are from
574 Chamberlain et al. (2013) and faded gray $\delta^{13}\text{C}_{\text{org}}$ values from Hu et al. (2015).

575 **Fig. 3:** Trace element concentration data from Qingshankou Member 1 and Qingshankou
576 Members 2 and 3 in the SK1-S core. Detrital proxies include the chemical index of alteration
577 (CIA). Redox thresholds for V/V+Ni are from Hatch and Leventhal (1992). Dashed lines in Mn
578 and V+Cr plots represent median concentrations. $\delta^{34}\text{S}_{\text{pyr}}$ data are from Huang et al. (2013).
579 Redox thresholds for Mo concentrations from Scott & Lyons (2012).

580 **Fig. 4:** Correlation of $\delta^{13}\text{C}_{\text{org}}$ time series from the Songliao Basin (*this study*) and Western
581 Interior Basin (N. America) (Joo & Sageman, 2014). Red lines represent Gaussian kernel
582 smoothed $\delta^{13}\text{C}_{\text{org}}$ values ($\sigma = \pm 150$ ka). The Songliao time scale derived from astronomical time
583 scale (Wu et al., 2013) anchored to a U/Pb zircon age date (Wang et al., 2016) (Sect. 3.1 and
584 appendix).

585 **Fig. 5:** Record of $\Delta^{13}\text{C}$ ($\delta^{13}\text{C}_{\text{carb}} - \delta^{13}\text{C}_{\text{org}}$) changes, approximating carbon isotope fractionation
586 across OAE3 in the Songliao Basin and Western Interior Basin (WIB) of North America. Red
587 lines represent Gaussian kernel smoothed $\Delta^{13}\text{C}$ values ($\sigma = \pm 150$ ka).

588 **Fig. 6:** Comparison of Os_i time series from the Songliao Basin SK1-S (green) and Demerara
589 Rise ODP Site 1259 (blue). Time scales from Songliao Basin (Wu et al., 2013; Wang et al.
590 2016), Demerara Rise (updated from Bornemann et al., 2008), and WIB (Joo and Sageman,
591 2014). Flood basalt emplacement in black (Wang et al., 2016a). Previously cited evidence for
592 the Qingshankou Formation marine incursions in yellow shaded intervals for presence of marine
593 biomarkers (Hu et al., 2015) and purple interval of $\delta^{34}\text{S}_{\text{pyr}}$ data (Huang et al., 2013).

594 **Fig. 7: a.)** Non-marine biogeochemical and depositional model of Qingshankou Member 1 also
595 depicting theoretical plots of density (ρ), salinity, total dissolved substances (TDS), and winter
596 and summer water temperature profiles. **b.)** Biogeochemical cycling and depositional model for
597 Qingshankou Members 2 and 3 during OAE3 interval. See text for discussion.

598 **References**

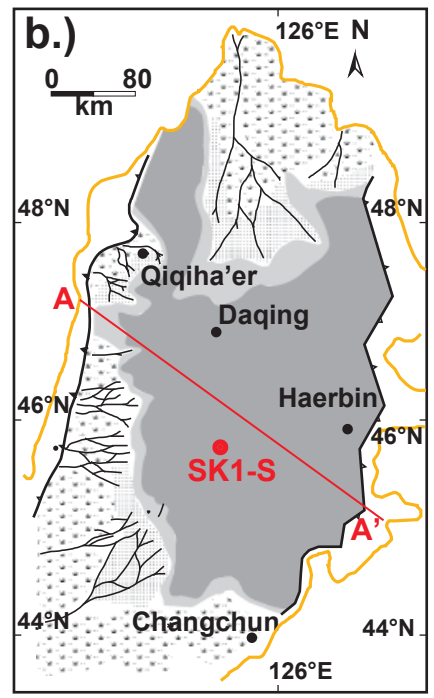
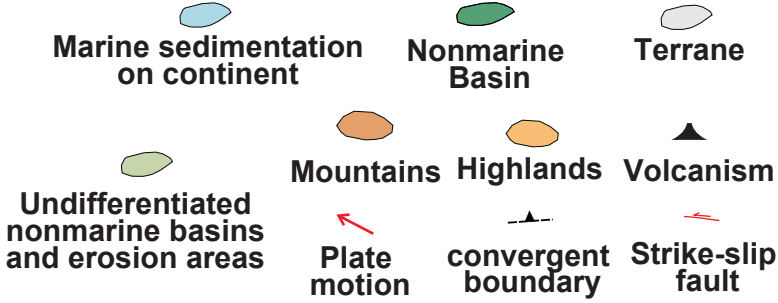
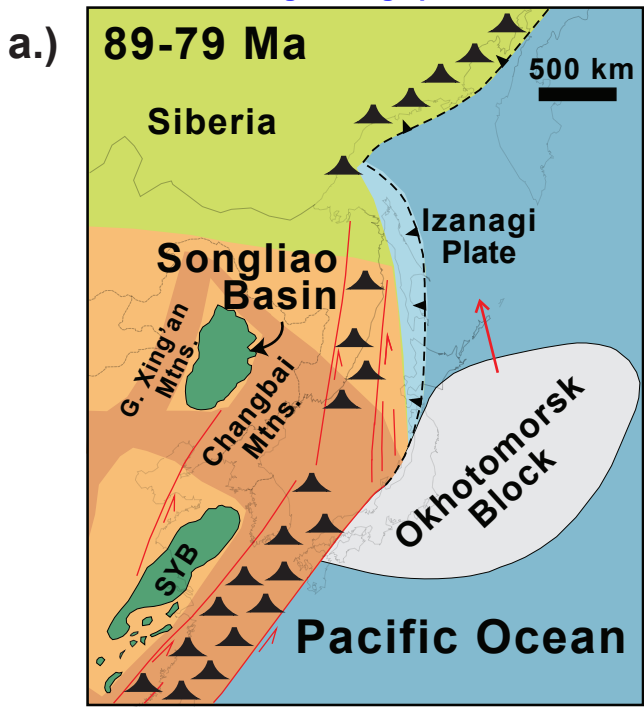
- 599 Algeo, T. J., Lyons, T. W., 2006. Mo–total organic carbon covariation in modern anoxic marine
600 environments: Implications for analysis of paleoredox and paleohydrographic conditions:
601 Paleocyanography. 21, 1
- 602 Alin, S.R., Johnson, T.C., 2007. Carbon cycling in large lakes of the world: A synthesis of production,
603 burial, and lake-atmosphere exchange estimates. *Global Biogeochem. Cycles*. 21
- 604 Arthur, M.A., Dean, W.E., Claypool, G.E., 1985. Anomalous C-13 enrichment in modern marine organic-
605 carbon. *Nature* 315, 216-218.
- 606 Arthur, M.A., Dean, W.E., Pratt, L.M., 1988. Geochemical and climatic effects of increased marine
607 organic-carbon burial at the Cenomanian-Turonian Boundary. *Nature* 335, 714-717.
- 608 Barclay, R.S., McElwain, J.C., Sageman, B.B., 2010. Carbon sequestration activated by a volcanic CO₂
609 pulse during Ocean Anoxic Event 2. *Nat Geosci* 3, 205-208.
- 610 Bechtel, A., Jia, J.L., Strobl, S.A.I., Sachsenhofer, R.F., Liu, Z.J., Gratzner, R., Puttmann, W., 2012.
611 Palaeoenvironmental conditions during deposition of the Upper Cretaceous oil shale sequences
612 in the Songliao Basin (NE China): Implications from geochemical analysis. *Organic Geochemistry*
613 46, 76-95.
- 614 Berner, R.A., 1982. Burial of organic-carbon and pyrite sulfur in the modern ocean – its geochemical
615 and environmental significance. *American Journal of Science* 282, 451-473.
- 616 Boehrer, B., Schultze, M., 2008. Stratification of lakes. *Rev. Geophys.* 46, 27.
- 617 Bornemann, A., Norris, R.D., Friedrich, O., Beckmann, B., Schouten, S., Damste, J.S.S., Vogel, J., Hofmann,
618 P., Wagner, T., 2008. Isotopic evidence for glaciation during the Cretaceous supergreenhouse.
619 *Science* 319, 189-192.
- 620 Calvert, S.E., Thode, H.G., Yeung, D., Karlin, R.E., 1996. A stable isotope study of pyrite formation in the
621 Late Pleistocene and Holocene sediments of the Black Sea. *Geochim Cosmochim Acta* 60, 1261-
622 1270.
- 623 Chamberlain, C.P., Wan, X., Graham, S.A., Carroll, A.R., Doebbert, A.C., Sageman, B.B., Blisniuk, P., Kent-
624 Corson, M.L., Wang, Z., Wang, C., 2013. Stable isotopic evidence for climate and basin evolution
625 of the Late Cretaceous Songliao basin, China. *Palaeogeography Palaeoclimatology Palaeoecology*
626 385, 106-124.
- 627 Cumming, V.M., Selby, D., Lillis, P.G., 2012. Re-Os geochronology of the lacustrine Green River
628 Formation: Insights into direct depositional dating of lacustrine successions, Re-Os systematics
629 and paleocontinental weathering. *Earth Planet Sc Lett* 359, 194-205.
- 630 Demaison, G., Moore, G.T., 1980. Anoxic environments and oil source bed genesis. *Organic*
631 *Geochemistry* 2, 9-31.
- 632 Du Vivier, A.D.C., Selby, D., Sageman, B.B., Jarvis, I., Groecke, D.R., Voigt, S., 2014. Marine Os-187/Os-
633 188 isotope stratigraphy reveals the interaction of volcanism and ocean circulation during
634 Oceanic Anoxic Event 2. *Earth Planet Sc Lett* 389, 23-33.
- 635 Feng, Z.-q., Jia, C.-z., Xie, X.-n., Zhang, S., Feng, Z.-h., Cross, T.A., 2010. Tectonostratigraphic units and
636 stratigraphic sequences of the nonmarine Songliao basin, northeast China. *Basin Research* 22,
637 79-95.
- 638 Gannoun, A., Burton, K.W., 2014. High precision osmium elemental and isotope measurements of North
639 Atlantic seawater. *Journal of Analytical Atomic Spectrometry* 29, 2330-2342.
- 640 Gao, Y., Wang, P., Cheng, R., Wang, G., Wan, X., Wu, H., Wang, S., Liang, W., 2009. Description of
641 Cretaceous Sedimentary Sequence of the First Member of the Qingshankou Formation
642 Recovered by CCSD-SK-1s Borehole in Songliao Basin: Lithostratigraphy, Sedimentary Facies, and
643 Cyclic Stratigraphy. *Earth Science Frontiers* 16, 314-323.

- 644 Glass, J.B., Orphan, V.J., 2012. Trace Metal Requirements for Microbial Enzymes Involved in the
645 Production and Consumption of Methane and Nitrous Oxide. *Frontiers in Microbiology* 3, 61.
- 646 Gomes, M.L., Hurtgen, M.T., 2013. Sulfur isotope systematics of a euxinic, low-sulfate lake: Evaluating
647 the importance of the reservoir effect in modern and ancient oceans. *Geology* 41, 663-666.
- 648 Graham, S.A., Hendrix, M.S., Johnson, C.L., Badamgarav, D., Badarch, G., Amory, J., Porter, M., Barsbold,
649 R., Webb, L.E., Hacker, B.R., 2001. Sedimentary record and tectonic implications of Mesozoic
650 rifting in southeast Mongolia. *Geological Society of America Bulletin* 113, 1560-1579.
- 651 Hatch, J.R., Leventhal, J.S., 1992. Relationship between inferred redox potential of the depositional
652 environment and geochemistry of the Upper Pennsylvanian (Missourian) Stark Shale Member of
653 the Dennis Limestone, Wabaunsee County, Kansas, U.S.A. *Chemical Geology* 99, 65-82.
- 654 Harris, N.B., Freeman, K.H., Pancost, R.D., White, T.S., and Mitchell, G.D., 2004. The character and origin
655 of lacustrine source rocks in the Lower Cretaceous synrift section, Congo Basin, west Africa.
656 *AAPG Bulletin* 88(8), 1163-1184
- 657 Hollander, D.J., Smith, M.A., 2001. Microbially mediated carbon cycling as a control on the delta C-13 of
658 sedimentary carbon in eutrophic Lake Mendota (USA): New models for interpreting isotopic
659 excursions in the sedimentary record. *Geochim Cosmochim Acta* 65, 4321-4337.
- 660 Hou, D., Li, M., Huang, Q., 2000. Marine transgressional events in the gigantic freshwater lake Songliao:
661 paleontological and geochemical evidence. *Organic Geochemistry* 31, 763-768.
- 662 Hu, J.F., Peng, P.A., Liu, M.Y., Xi, D.P., Song, J.Z., Wan, X.Q., Wang, C.S., 2015. Seawater Incursion Events
663 in a Cretaceous Paleo-lake Revealed by Specific Marine Biological Markers. *Scientific Reports* 5,
664 9508.
- 665 Huang, Y.J., Yang, G.S., Gu, J., Wang, P.K., Huang, Q.H., Feng, Z.H., Feng, L.J., 2013. Marine incursion
666 events in the Late Cretaceous Songliao Basin: Constraints from sulfur geochemistry records.
667 *Palaeogeography Palaeoclimatology Palaeoecology* 385, 152-161.
- 668 Jarvis, I., Gale, A.S., Jenkyns, H.C., Pearce, M.A., 2006. Secular variation in Late Cretaceous carbon
669 isotopes: a new delta C-13 carbonate reference curve for the Cenomanian-Campanian (99.6-
670 70.6 Ma). *Geological Magazine* 143, 561-608.
- 671 Jarvis, I., Lignum, J.S., Groecke, D.R., Jenkyns, H.C., Pearce, M.A., 2011. Black shale deposition,
672 atmospheric CO₂ drawdown, and cooling during the Cenomanian-Turonian Oceanic Anoxic
673 Event. *Paleoceanography* 26.
- 674 Jenkyns, H.C., 2010. Geochemistry of oceanic anoxic events. *Geochemistry Geophysics Geosystems* 11.
- 675 Joo, Y.J., Sageman, B.B., 2014. Cenomanian to Campanian carbon isotope chemostratigraphy from the
676 Western Interior Basin, USA. *Journal of Sedimentary Research* 84, 529-542.
- 677 Kump, L.R., Arthur, M.A., 1999. Interpreting carbon-isotope excursions: carbonates and organic matter.
678 *Chemical Geology* 161, 181-198.
- 679 Kuroda, J., Jiménez-Espejo, F.J., Nozaki, T., Gennari, R., Lugli, S., Manzi, V., Roveri, M., Flecker, R., Sierro,
680 F.J., Yoshimura, T., Suzuki, K., Ohkouchi, N., 2016. Miocene to Pleistocene osmium isotopic
681 records of the Mediterranean sediments. *Paleoceanography* 31, 148-166.
- 682 Locklair, R., Sageman, B., Lerman, A., 2011. Marine carbon burial flux and the carbon isotope record of
683 Late Cretaceous (Coniacian-Santonian) Oceanic Anoxic Event III. *Sedimentary Geology* 235, 38-
684 49.
- 685 Locklair, R.E., Sageman, B.B., 2008. Cyclostratigraphy of the Upper Cretaceous Niobrara Formation,
686 Western Interior, USA: A Coniacian-Santonian orbital timescale. *Earth Planet Sc Lett* 269, 539-
687 552.
- 688 Ludvigson, G.A., Joeckel, R.M., González, L.A., Gulbranson, E.L., Rasbury, E.T., Hunt, G.J., Kirkland, J.I.,
689 Madsen, S., 2010. Correlation of Aptian-Albian Carbon Isotope Excursions in Continental Strata
690 of the Cretaceous Foreland Basin, Eastern Utah, U.S.A. *Journal of Sedimentary Research* 80, 955.

- 691 Lowery, C.M., Leckie, R.M., Sageman, B.B., 2017. Micropaleontological evidence for redox changes in the
692 OAE3 interval of the US Western Interior: Global vs. local processes. *Cretaceous Research* 69,
693 34-48.
- 694 Maberly, S.C., Barker, P.A., Stott, A.W., De Ville, M.M., 2013. Catchment productivity controls CO₂
695 emissions from lakes. *Nat. Clim. Chang.* 3, 391-394.
- 696 MacLeod, K.G., Huber, B.T., Jimenez Berrocoso, A., Wendler, I., 2013. A stable and hot Turonian without
697 glacial delta O-18 excursions is indicated by exquisitely preserved Tanzanian foraminifera.
698 *Geology* 41, 1083-1086.
- 699 Meyers, P.A., 1994. Preservation of elemental and isotopic source identification of sedimentary organic-
700 matter. *Chemical Geology* 114, 289-302.
- 701 Moldowan, J.M., Fago, F.J., Lee, C.Y., Jacobson, S.R., Watt, D.S., Slougui, N.-E., Jeganathan, A., Young,
702 D.C., 1990. Sedimentary 24-n-Propylcholestanes, Molecular Fossils Diagnostic of Marine Algae.
703 *Science* 247, 309-312.
- 704 Nesbitt, H.W., Young, G.M., 1982. Early Proterozoic climates and plate motions inferred from major
705 element chemistry of lutites. *Nature* 299, 715-717.
- 706 Oxburgh, R., 2001. Residence time of osmium in the oceans. *Geochemistry, Geophysics, Geosystems* 2.
707 Pagani, M., Huber, M., Sageman, B., 2014. 6.13 - Greenhouse Climates A2 - Holland, Heinrich D, in:
708 Turekian, K.K. (Ed.), *Treatise on Geochemistry (Second Edition)*. Elsevier, Oxford, pp. 281-304.
- 709 Peucker-Ehrenbrink, B., Ravizza, G., 2000. The marine osmium isotope record. *Terra Nova* 12, 205-219.
- 710 Poirier, A., Hillaire-Marcel, C., 2011. Improved Os-isotope stratigraphy of the Arctic Ocean. *Geophys Res*
711 *Lett* 38, n/a-n/a.
- 712 Rooney, A.D., Selby, D., Lloyd, J.M., Roberts, D.H., Lückge, A., Sageman, B.B., Prouty, N.G., 2016. Tracking
713 millennial-scale Holocene glacial advance and retreat using osmium isotopes: Insights from the
714 Greenland ice sheet. *Quaternary Science Reviews* 138, 49-61.
- 715 Sageman, B.B., Lyons, T.W., Joo, Y.J., 2014a. 9.6 - Geochemistry of Fine-Grained, Organic Carbon-Rich
716 Facies A2 - Holland, Heinrich D, in: Turekian, K.K. (Ed.), *Treatise on Geochemistry (Second*
717 *Edition)*. Elsevier, Oxford, pp. 141-179.
- 718 Sageman, B.B., Singer, B.S., Meyers, S.R., Siewert, S.E., Walaszczyk, I., Condon, D.J., Jicha, B.R.,
719 Obradovich, J.D., Sawyer, D.A., 2014b. Integrating Ar-40/Ar-39, U-Pb, and astronomical clocks in
720 the Cretaceous Niobrara Formation, Western Interior Basin, USA. *Geological Society of America*
721 *Bulletin* 126, 956-973.
- 722 Scholle, P.A., Arthur, M.A., 1980. Carbon isotope fluctuations in Cretaceous pelagic limestones -
723 potential stratigraphic and petroleum exploration tool. *AAPG Bulletin* 64, 67-87.
- 724 Scott, C., Lyons, T.W., 2012. Contrasting molybdenum cycling and isotopic properties in euxinic versus
725 non-euxinic sediments and sedimentary rocks: Refining the paleoproxies. *Chemical Geology* 324,
726 19-27.
- 727 Selby, D., Creaser, R.A., 2003. Re-Os geochronology of organic rich sediments: an evaluation of organic
728 matter analysis methods. *Chemical Geology* 200, 225-240.
- 729 Talbot, M. R., 1990, A review of the palaeohydrological interpretation of carbon and oxygen isotopic
730 ratios in primary lacustrine carbonates: *Chemical Geology: Isotope Geoscience section*, v. 80, no.
731 4, p. 261-279.
- 732 Talbot, M.R., Jensen, N.B., Lærdal, T. and Filippi, M.L., 2006. Geochemical responses to a major
733 transgression in giant African lakes. *Journal of Paleolimnology* 35, 467-489.
- 734 Tessin, A., Hendy, I., Sheldon, N., Sageman, B., 2015. Redox-controlled preservation of organic matter
735 during "OAE 3" within the Western Interior Seaway. *Paleoceanography* 30, 702-717.
- 736 Tribovillard, N., Algeo, T.J., Lyons, T., Riboulleau, A., 2006. Trace metals as paleoredox and
737 paleoproductivity proxies: An update. *Chemical Geology* 232, 12-32.

- 738 Turgeon, S.C., Creaser, R.A., 2008. Cretaceous oceanic anoxic event 2 triggered by a massive magmatic
739 episode. *Nature* 454, 323-U329.
- 740 Wagreich, M., 2012. "OAE 3" - regional Atlantic organic carbon burial during the Coniacian-Santonian.
741 *Climate of the Past* 8, 1447-1455.
- 742 Wan, X., Zhao, J., Scott, R.W., Wang, P., Feng, Z., Huang, Q., Xi, D., 2013. Late Cretaceous stratigraphy,
743 Songliao Basin, NE China: SK1 cores. *Palaeogeography Palaeoclimatology Palaeoecology* 385, 31-
744 43.
- 745 Wang, C.S., Feng, Z.G., Zhang, L.M., Huang, Y.J., Cao, K., Wang, P.J., Zhao, B., 2013. Cretaceous
746 paleogeography and paleoclimate and the setting of SK1 borehole sites in Songliao Basin,
747 northeast China. *Palaeogeography Palaeoclimatology Palaeoecology* 385, 17-30.
- 748 Wang, P.J., Gao, Y., Cheng, R., Wang, G., Wu, H., Wan, X., Yang, G., Wang, Z., 2009. Description of
749 Cretaceous Sedimentary Sequence of the Second and Third Member of the Qingshankou
750 Formation Recovered by CCSD-SK-1s Borehole in Songliao Basin: Lithostratigraphy, Sedimentary
751 Facies and Cyclic Stratigraphy. *Earth Science Frontiers* 16, 288-313.
- 752 Wang, P.J., Mattern, F., Didenko, N.A., Zhu, D.F., Singer, B., Sun, X.M., 2016a. Tectonics and cycle system
753 of the Cretaceous Songliao Basin: An inverted active continental margin basin. *Earth-Science*
754 *Reviews* 159, 82-102.
- 755 Wang, T., Ramezani, J., Wang, C., Wu, H., He, H., Bowring, S.A., 2016b. High-precision U–Pb
756 geochronologic constraints on the Late Cretaceous terrestrial cyclostratigraphy and
757 geomagnetic polarity from the Songliao Basin, Northeast China. *Earth Planet Sc Lett* 446, 37-44.
- 758 Wedepohl, K.H., 1971. Environmental influences on the chemical composition of shales and clays.
759 *Physics and Chemistry of the Earth* 8, 307-333.
- 760 Wendler, I., 2013. A critical evaluation of carbon isotope stratigraphy and biostratigraphic implications
761 for Late Cretaceous global correlation. *Earth-Science Reviews* 126, 116-146.
- 762 Wu, H., Zhang, S., Jiang, G., Hinnov, L., Yang, T., Li, H., Wan, X., Wang, C., 2013. Astrochronology of the
763 Early Turonian–Early Campanian terrestrial succession in the Songliao Basin, northeastern China
764 and its implication for long-period behavior of the Solar System. *Palaeogeography*
765 *Palaeoclimatology Palaeoecology* 385, 55-70.
- 766 Wunsche, L., Gulacar, F.O., Buchs, A., 1987. Several unexpected marine sterols in a fresh-water
767 sediment. *Organic Geochemistry* 11, 215-219.
- 768 Xi, D.P., Cao, W.X., Huang, Q.H., Do Carmo, D.A., Li, S., Jing, X., Tu, Y.J., Jia, J.Z., Qu, H.Y., Zhao, J., Wan,
769 X.Q., 2016. Late Cretaceous marine fossils and seawater incursion events in the Songliao Basin,
770 NE China. *Cretaceous Research* 62, 172-182.
- 771 Xu, W., Ruhl, M., Jenkyns, H.C., Hesselbo, S.P., Riding, J.B., Selby, D., Naafs, B.D.A., Weijers, J.W.H.,
772 Pancost, R.D., Tegelaar, E.W., Idiz, E.F., 2017. Carbon sequestration in an expanded lake system
773 during the Toarcian oceanic anoxic event. *Nature Geosci* advance online publication.
- 774 Yang, Y.T., 2013. An unrecognized major collision of the Okhotomorsk Block with East Asia during the
775 Late Cretaceous, constraints on the plate reorganization of the Northwest Pacific. *Earth-Science*
776 *Reviews* 126, 96-115.
- 777 Zhao, J., Wan, X.Q., Xi, D.P., Jing, X., Li, W., Huang, Q.H., Zhang, J.Y., 2014. Late Cretaceous palynology
778 and paleoclimate change: Evidence from the SK1 (South) core, Songliao Basin, NE China. *Sci.*
779 *China-Earth Sci.* 57, 2985-2997.

Figure1
[Click here to download Figure: Fig1.pdf](#)



Qingshankou Fm. - Member 1

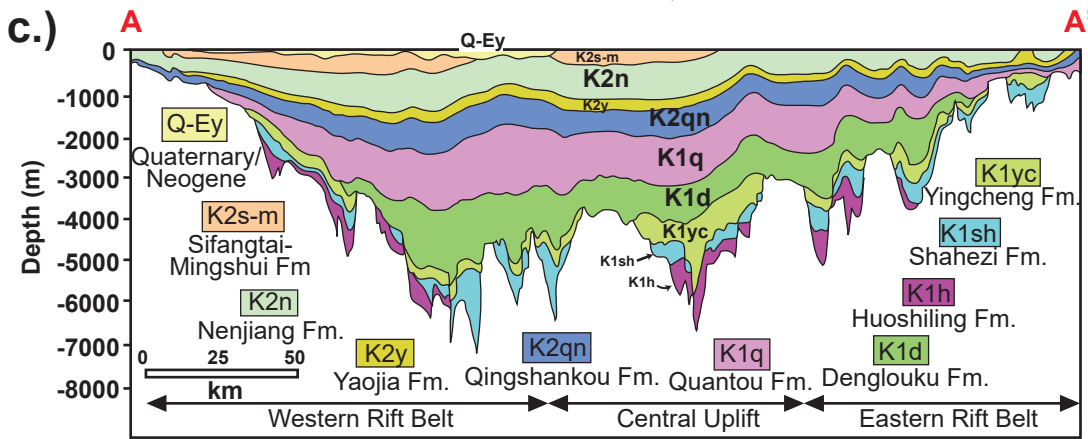
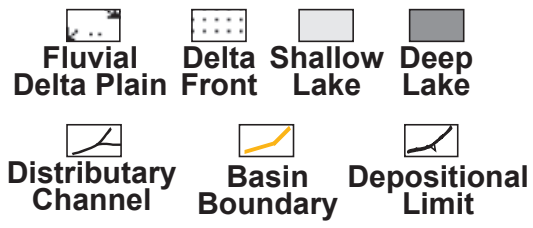


Figure 2
Click here to download Figure: Fig2.pdf

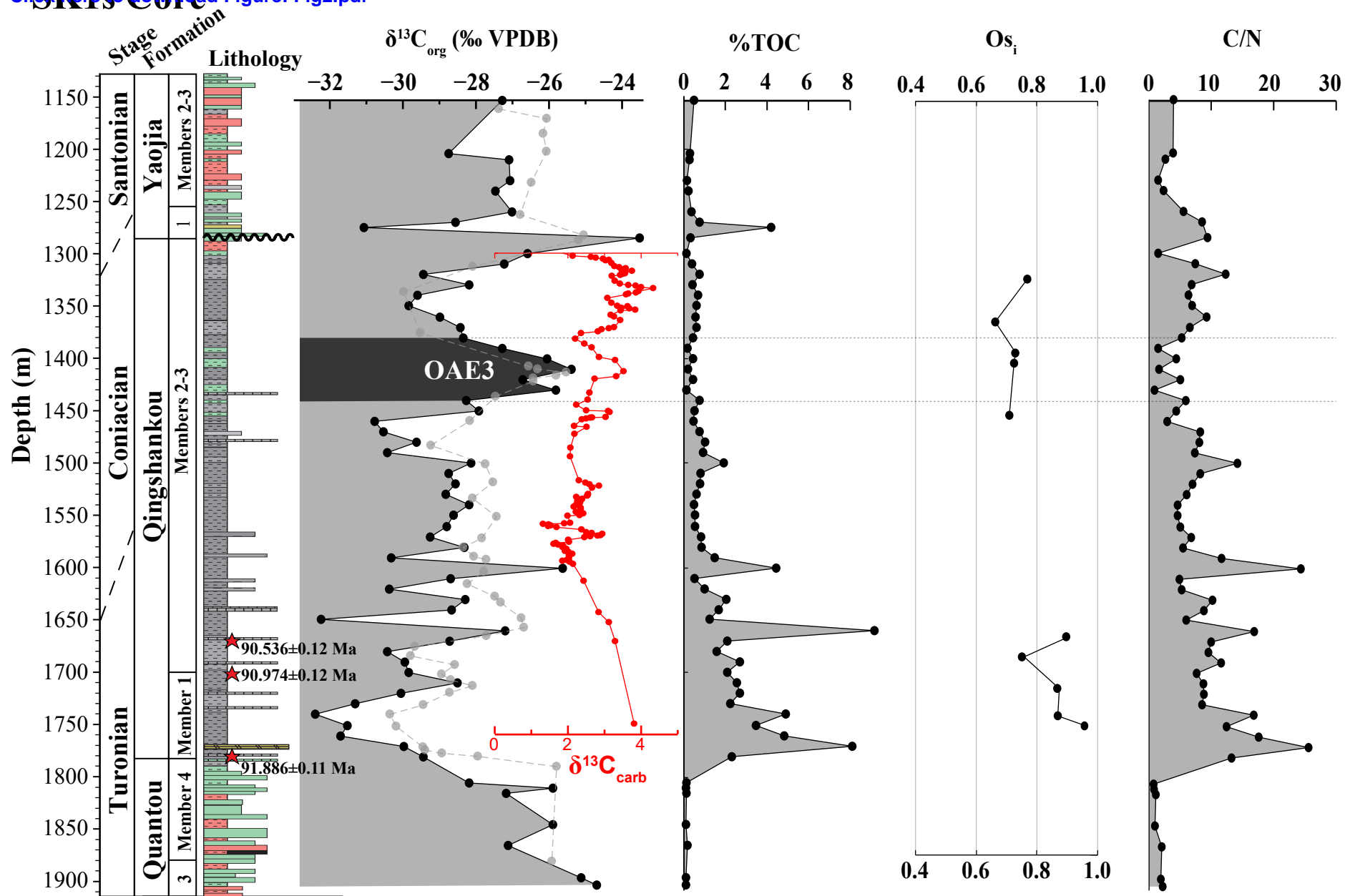


Figure 3

[Click here to download Figure: Fig3.pdf](#)

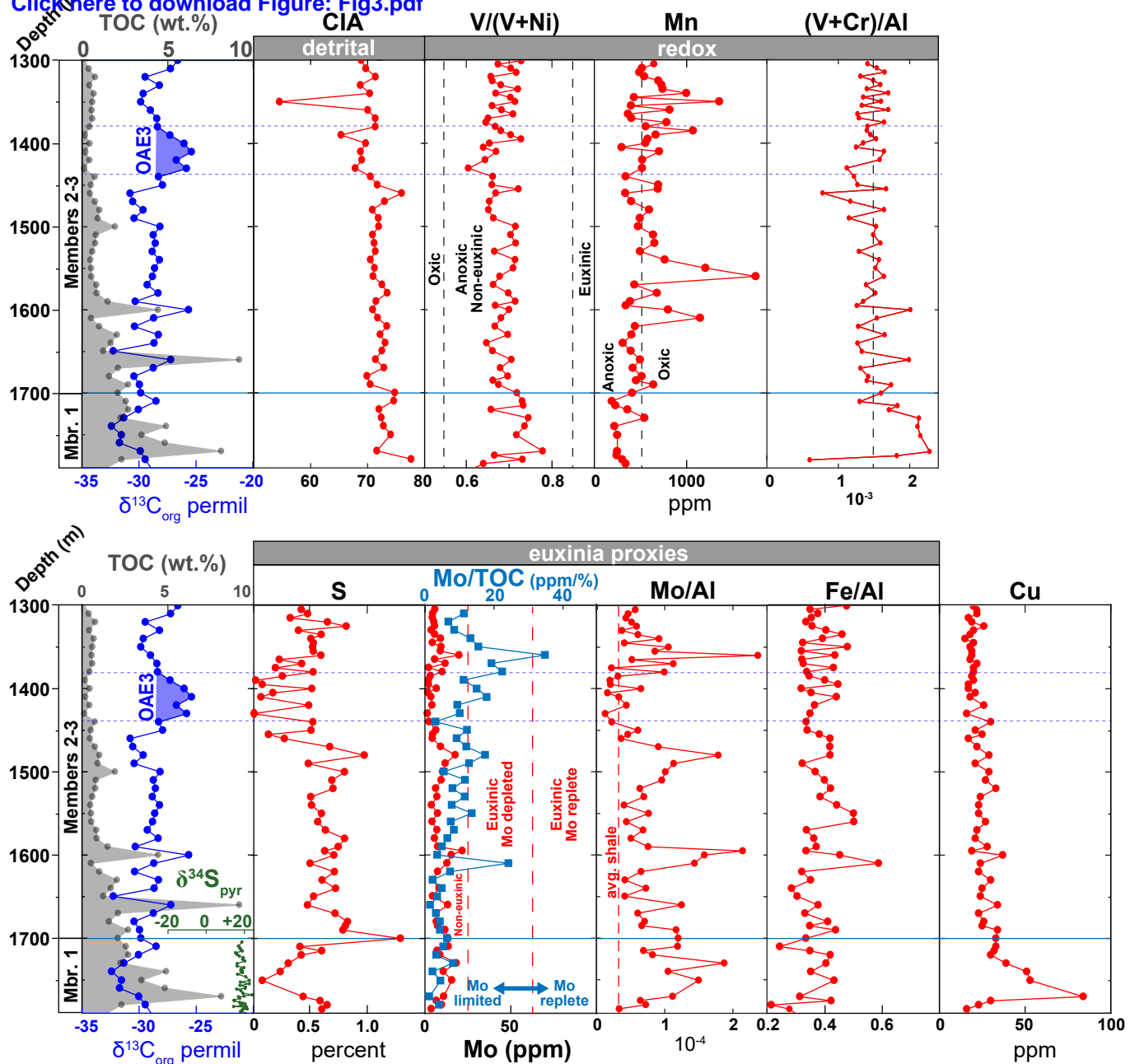


Figure5

[Click here to download Figure_Fig5.pdf](#)

Songhao Basin

Angus Aristocrat Core (WIB)

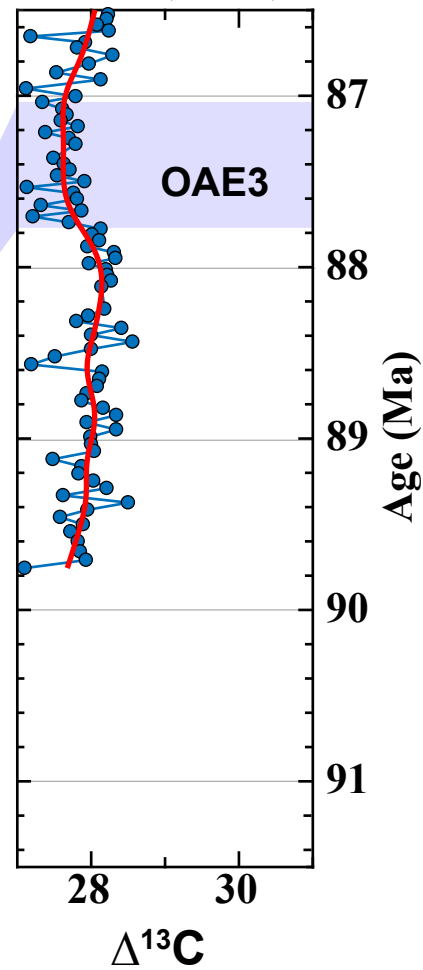
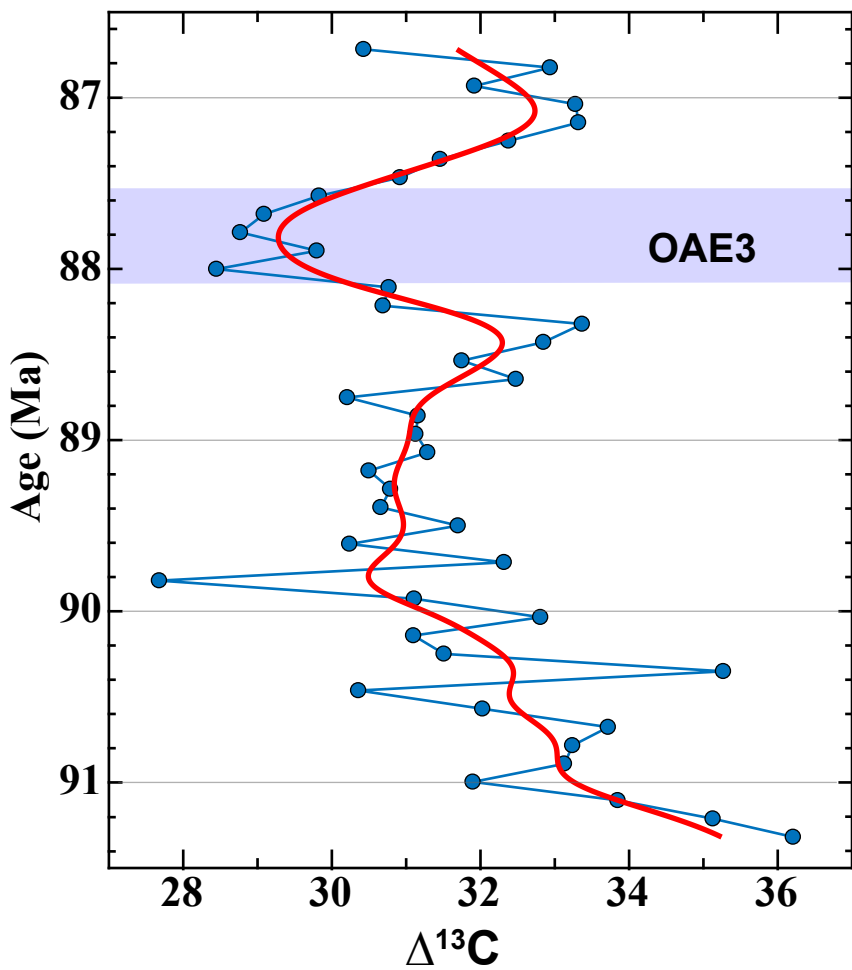


Figure6

[Click here to download Figure: Fig6.pdf](#)

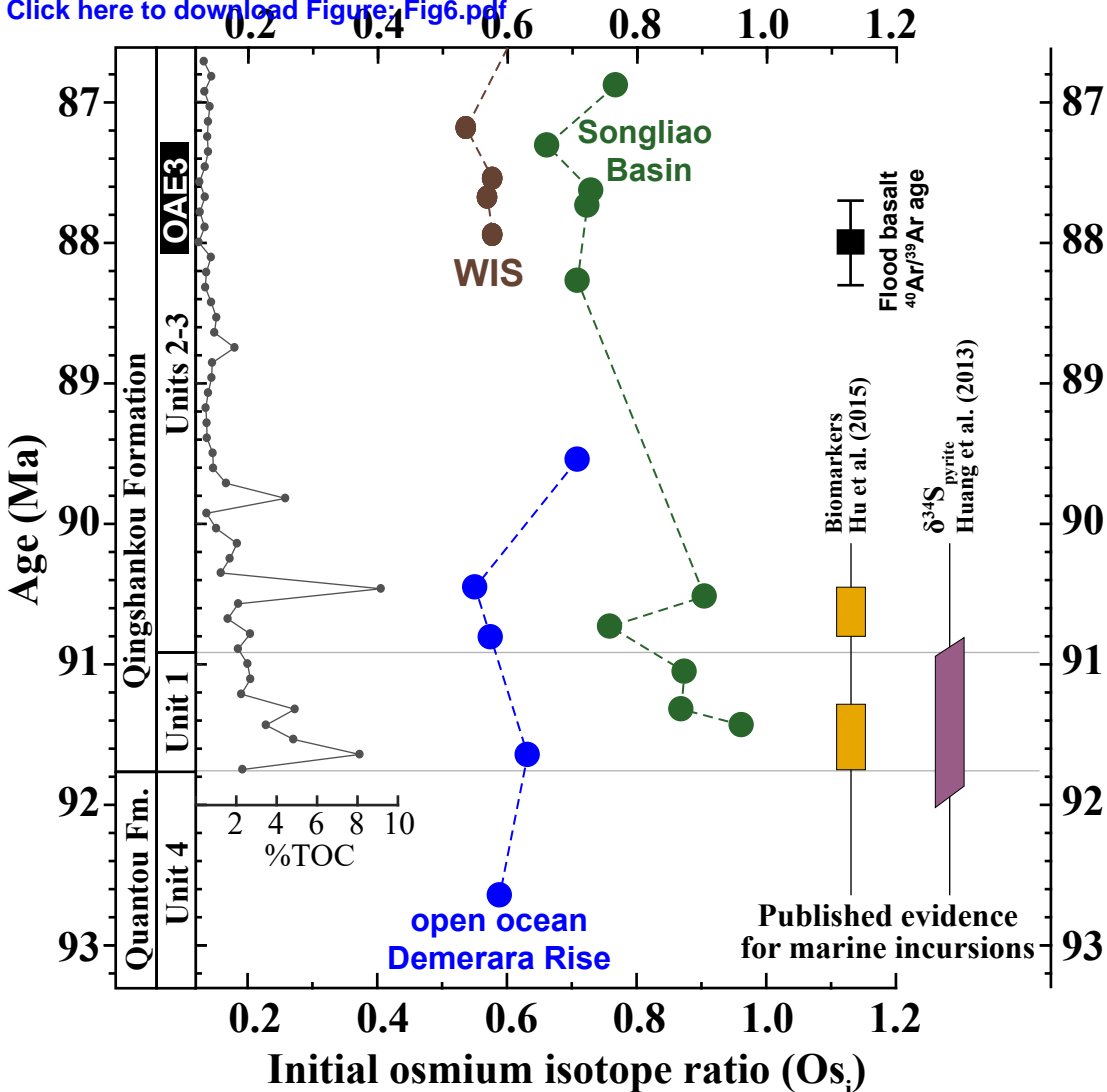
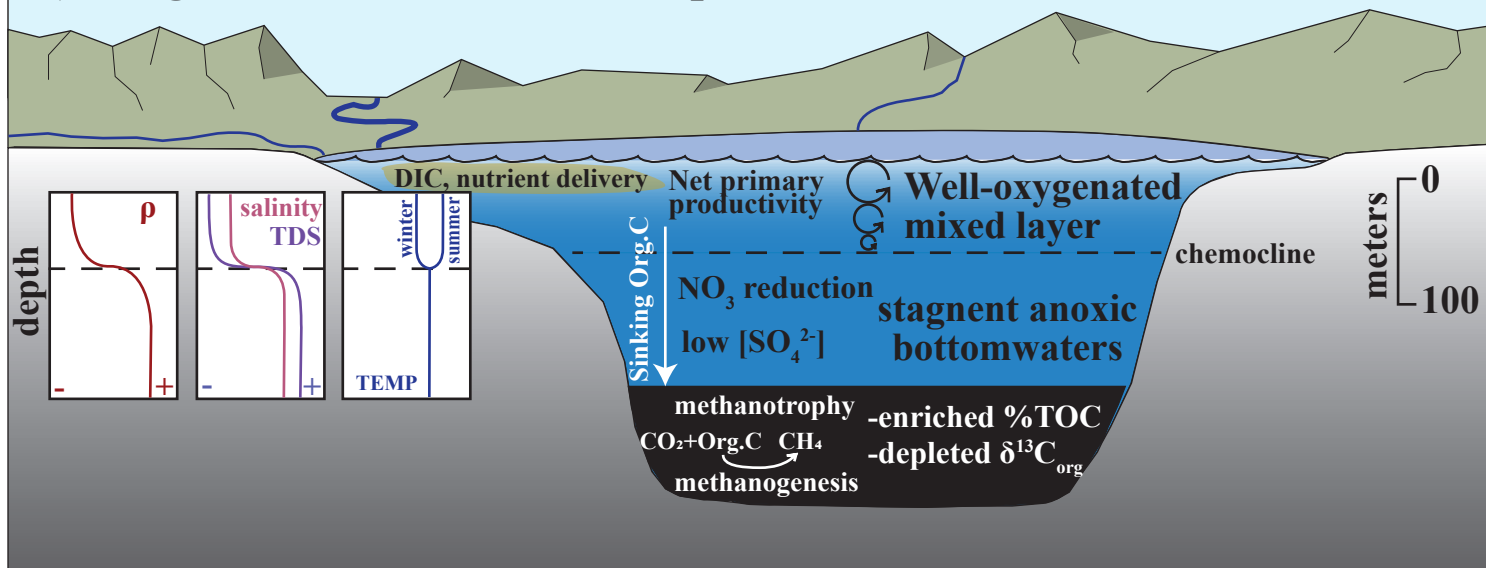


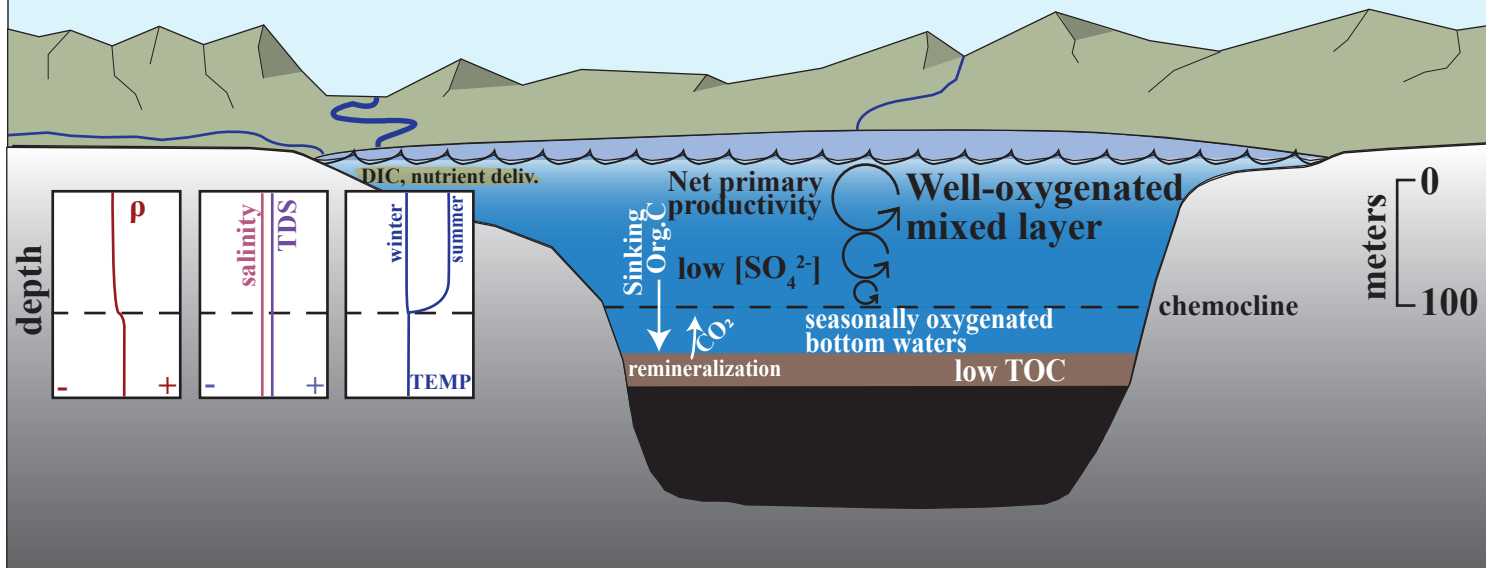
Figure7

[Click here to download Figure: Fig7.pdf](#)

a.) Qingshankou Member 1: Deep meromictic lake



b.) Qingshankou Members 2-3 (OAE 3): oxygenated bottom waters



Revised appendix

[Click here to download Supplementary material for online publication only: Jonesetal_Appendix_revised.docx](#)

Supplementary material table A1

[Click here to download Supplementary material for online publication only: AppendixTable1_GeochemData.xlsx](#)

Supplementary material table A2

[Click here to download Supplementary material for online publication only: AppendixTable2_XRFdata.xlsx](#)